



the gravitational mass  $M$  and the rest mass  $m$  of the thin shell in a certain parameter range. After that, we follow [36, 37] to analyze the bouncing behavior of the thin shell on the Penrose diagram. The consequence of this behavior is that the thin shell would not form singularity ultimately after collapsing to form a black hole, therefore it is worth to remind that the bouncing behavior is not an observational effect for exterior observers. Besides, the motion of the thin shell in higher dimensions is also analyzed. Furthermore, the weak cosmic censorship conjecture is tested and turns out to hold in this model.

The paper is organized as follows: In Sec. II, we introduce the bouncing behavior of collapsing dust star in 4D EGB. Then we are motivated to study collapsing shells and obtain the EOM of spherical thin shells in  $D$  dimensions in Sec. III. In Sec. IV, we study in detail the EOM of thin shells both in four and higher dimensions. In Sec. V, we test the weak cosmic censorship in this model. Finally, some concluding remarks will be presented in Sec. VI.

## II. DUST COLLAPSE IN THE NOVEL 4D EGB GRAVITY

In this section, we review the process of gravitational collapse in four dimensional EGB gravity and show the existence of bouncing behavior for collapsing dust star. Note that dust collapse in 4D EGB gravity has been studied in [3], but they restricted on marginally bound collapse of dust star so that the bouncing behavior was not considered. Since the surface of a dust star follows geodesics of test particles with respect to the external spacetime (4D EGB black hole) [3], we focus on the geodesics instead of analyzing the trajectory of collapsing dust star directly here.

We first introduce the formalism of four dimensional EGB gravity. Consider  $D \geq 5$  dimensional EGB theory which has action

$$S_M = \frac{1}{16\pi G_d} \int d^D x \sqrt{-g} (R + \alpha L_{GB}),$$

where the Gauss-Bonnet term  $L_{GB}$  is defined by

$$L_{GB} = R^2 - 4R_{ab}R^{ab} + R^{abcd}R_{abcd}.$$

For this theory, the spherically symmetric vacuum solution has given by Boulware and Deser [38],

$$ds^2 = -H(r)dt^2 + \frac{dr^2}{H(r)} + r^2 d\Omega_{D-2}^2, \quad (1)$$

where  $d\Omega_{D-2}^2$  is the line element of the unit  $S^{D-2}$  and

$$H(r) = 1 + \frac{r^2}{2\tilde{\alpha}} \left( 1 - \sqrt{1 + \frac{16\tilde{\alpha}M}{(D-2)r^{D-1}}} \right),$$

where  $\tilde{\alpha} = (D-3)(D-4)\alpha$ .

The recent proposal of 4D EGB [1] extend (1) to  $D = 4$  and gives four dimensional EGB vacuum solution, namely

$$ds^2 = -F(r)dt^2 + \frac{dr^2}{F(r)} + r^2 (d\theta^2 + \sin^2 \theta d\phi^2), \quad (2)$$

where

$$F(r) = 1 + \frac{r^2}{2\alpha} \left( 1 - \sqrt{1 + \frac{8\alpha M}{r^3}} \right),$$

then  $F(r) = 0$  gives the event horizons of 4D EGB black hole, namely

$$r_{\pm} = M \pm \sqrt{M^2 - \alpha}. \quad (3)$$

Notice that (2) is well-defined when  $r \rightarrow 0$ , while a straight-forward calculation shows, as  $r \rightarrow 0$ , the scalar  $R^{abcd}R_{abcd}$  diverge as  $\frac{M\alpha}{r^3}$ , therefore  $r = 0$  is a real singularity.

Next we show the existence of bouncing behavior for a test particle which is freely falling in 4D EGB gravity. In this section, we restrict ourself to non-extremal cases, i.e. both  $r_+$  and  $r_-$  in (3) exist.

The radial geodesic equation is given by

$$g_{rr} \left( \frac{dr}{d\tau} \right)^2 + g_{tt} \left( \frac{dt}{d\tau} \right)^2 = -1 \quad (4)$$

and consider the conserved quantities associated with the Killing vectors  $\partial_t$ , there is

$$E = -p_t = -g_{tt}p^t = -g_{tt} \frac{dt}{d\tau}. \quad (5)$$

Combine (4) with (5), we obtain

$$\left( \frac{dr}{d\tau} \right)^2 = E^2 - F(r), \quad (6)$$

which tells us that the physical region of trajectory of test particle should be confined in  $E^2 - F(r) \geq 0$ . Due to  $F(r \rightarrow 0) = 1$ , test particle with  $E \in [0, 1)$  must be bounced back before reaching  $r = 0$ .

By analyzing the geodesic of test particle in 4D EGB black hole background, we conclude that there exist bouncing behavior for collapsing dust star. We then ask, the bouncing behavior is a universal phenomenon for self-gravitational collapsing system in 4D EGB theory? To explore this issue further, we are motivated to explore the trajectory of collapsing thin spherical shell in this theory.

## III. THE EQUATION OF MOTION OF THIN SHELL IN D DIMENSION

In this paper, the model is based on a  $D$  dimensional spherically symmetric spacetime  $M$  which is split into two segments by a timelike hypersurface  $\Sigma$ , whose two

sides will be denoted  $\Sigma_{\pm}$ , the hypersurfaces can then be treated as the boundary of each half of the spacetime. Varying the action gives the generalized Israel junction conditions [39] on  $\Sigma$ , which has been strictly re-derived by expressing the field equations in terms of distributions recently [40]. Note that the hypersurface describes the evolution of a thin spherical shell. Our goal is to derive the shell's EOM under junction conditions and the shell's equation of state. To start with, we consider  $D$  dimensional EGB theory with spherically symmetric thin shell, whose action is given by

$$\begin{aligned} S &= S_M + S_{matter} \\ &= \frac{1}{16\pi G_D} \int_M d^D x \sqrt{-g} (R + \alpha L_{GB}) \\ &\quad - \int_{\Sigma} d^{D-1} x \sqrt{-h} L_m^{\Sigma}, \end{aligned} \quad (7)$$

where  $h_{ab}$  is the induced metric on  $\Sigma$ .

Like Einstein case, it's necessary to add a surface term to (7) in order to have a well-defined variational problem, the corresponding term is

$$S_{\Sigma} = -\frac{1}{8\pi G_D} \int_{\Sigma_{\pm}} d^{D-1} x \sqrt{-h} \left\{ K + 2\alpha \left( J - 2\hat{G}^{ab} K_{ab} \right) \right\},$$

where  $\hat{G}^{ab}$  is the Einstein tensor related to  $h_{ab}$ ,  $J$  is the trace of  $J_{ab}$  which defined as

$$\begin{aligned} J_{ab} &= \frac{1}{3} (2K K_{ac} K_b^c + K_{cd} K^{cd} K_{ab} \\ &\quad - 2K_{ac} K^{cd} K_{db} - K^2 K_{ab}), \end{aligned}$$

where  $K$  is the trace of extrinsic curvature and the extrinsic curvature of thin shell is given by <sup>1</sup>

$$K_{ab} = h_a^{\mu} h_b^{\nu} \nabla_{\mu} n_{\nu}, \quad (8)$$

where  $n^{\nu}$  is the normal vector of thin shell.

As an aid to derive junction conditions, we introduce Gaussian normal coordinates in the neighborhood of  $\Sigma$ . We write the metric  $g_{\mu\nu}$  has the form

$$\begin{aligned} ds^2 &= d\omega^2 + h_{ab} dx^a dx^b \\ &= d\omega^2 - n^2(\omega, \tau) d\tau^2 + \sum_{i=1}^{D-2} \frac{r^2(\omega, \tau)}{\left(1 + \frac{1}{4} \sum_{j=1}^{D-2} x_j^2\right)^2} dx_i^2 \end{aligned} \quad (9)$$

and the extrinsic curvature of surfaces  $\omega = \text{constant}$  is  $K_{ab} = -\frac{1}{2} \partial_{\omega} h_{ab}$ . Substituting the metric ansatz (9) into  $S_{tot} = S + S_{\Sigma}$ , then  $S_{tot}$  reduce to the following form

$$\begin{aligned} S_{reduced} &= \frac{A_{D-2}}{16\pi G_D} \left\{ \int d\omega d\tau (D-2) n r^{D-3} \left( -2\dot{\omega}^2 r \right. \right. \\ &\quad + (-3+D) \frac{\psi}{r} + \frac{4\tilde{\alpha}}{r^2} \left( -\psi \dot{\omega}^2 r + \frac{1}{2r} (-5+D) \left( \frac{1}{2} - (\partial_{\omega} r)^2 \right. \right. \\ &\quad \left. \left. - \frac{\dot{r}^2}{n^2} \left( \psi + \frac{7\dot{r}^2}{6n^2} \right) + \frac{1}{2} (\partial_{\omega} r)^4 \right) \right) \left. \right\} \\ &\quad + \int_{\Sigma_{\pm}} d\tau 2n(D-2)r^{D-3} \partial_{\omega} r \left( 1 + \frac{2\tilde{\alpha}}{r^2} \left( \psi + \frac{2}{3} (\partial_{\omega} r)^2 \right) \right) \\ &\quad - \int_{\Sigma} d^{D-1} x \sqrt{-h} L_m^{\Sigma}, \end{aligned} \quad (10)$$

where  $A_{D-2} = \frac{2\pi^{\frac{D-1}{2}}}{\Gamma[\frac{D-1}{2}]}$  is the area of unit  $S^{D-2}$ ,  $\dot{r}$  denotes  $\partial_{\tau} r$  and

$$\psi = 1 - \frac{\dot{r}^2}{n^2} - (\partial_{\omega} r)^2.$$

Varying the reduced action (10), one can obtain junction condition

$$\begin{aligned} &\frac{(D-2)}{n^2} \left[ K_i^i \left( 1 + 2\tilde{\alpha} \left( \frac{1}{r^2} + \frac{\dot{r}^2}{n^2 r^2} - \frac{1}{3} (K_i^i)^2 \right) \right) \right]_{-}^{+} \\ &= -8\pi G_D S^{\tau\tau} < +\infty, \end{aligned} \quad (11)$$

where  $[X]_{-}^{+} \doteq X_{+} - X_{-}$  (we have chosen the normal vector of  $\Sigma$  to be outward-pointing, i.e pointing from the inside of shell to outside) and the energy-momentum tensor is defined by

$$S^{ab} = \frac{2}{\sqrt{-h}} \frac{\delta S_{matter}}{\delta h_{ab}}.$$

Note that  $K_i^i = \frac{1}{D-2} H^{ij} K_{ij}$ , where  $H_{ij} dx^i dx^j = h_{ab} dx^a dx^b + n^2(\omega, \tau) d\tau^2$ .

Suppose the velocity of an comoving observer on the radial collapsing thin shell to be  $u^a = (\partial_{\tau})^a$ , where  $\tau$  is the proper time of the observer, then the metric of the shell has the form

$$ds_{D-1}^2 = -d\tau^2 + r^2(\tau) d\Omega_{D-2}^2. \quad (12)$$

Assuming that the shell satisfy pressureless condition, then its surface energy momentum has

$$S^{ab} = \sigma(\tau) u^a u^b, \quad (13)$$

where  $\sigma$  denote surface density. From the conservation equations  ${}^{(D-1)}\nabla_b S_a^b = 0$ , where  ${}^{(D-1)}\nabla_b$  is the derivative operator on  $\Sigma$ , we obtain

$$\frac{\dot{\sigma}}{\sigma} + (D-2) \frac{\dot{r}}{r} = 0. \quad (14)$$

The rest mass of shell is defined as  $m = \sigma A_{D-2} r^{D-2}$  and (14) would implies  $m$  is a constant.

<sup>1</sup>  $\mu, \nu$  are the indexes of coordinates of spacetime, while  $a, b$  are the indexes of coordinates of  $\Sigma$ .

Since we consider a thin shell, vacuum condition holds in inner and outside of the shell, therefore the metric of bulk is given by

$$ds^2 = -f(r)dt^2 + \frac{dr^2}{f(r)} + r^2 d\Omega_{D-2}^2, \quad (15)$$

where

$$f(r) \equiv f_-(r) = 1;$$

$$f(r) \equiv f_+(r) = 1 + \frac{r^2}{2\tilde{\alpha}} \left( 1 - \sqrt{1 + \frac{16\tilde{\alpha}M}{(D-2)r^{D-1}}} \right).$$

Because both sides must have the same induced metric on the shell, then we have

$$ds_\Sigma^2 = \left( -f_\pm(r)\dot{t}^2 + \frac{1}{f_\pm(r)}\dot{r}^2 \right) d\tau^2 + r^2(\tau) d\Omega_{D-2}^2,$$

where

$$-f_\pm(r)\dot{t}^2 + \frac{1}{f_\pm(r)}\dot{r}^2 = -1. \quad (16)$$

The equation (16) means if we know the  $r(\tau)$ , then we would obtain  $t(\tau)$  so that the spherical shell motion  $r(t)$  is clear for observer at infinity.

Now we define the hypersurface  $\Sigma$  as  $r = r(\tau)$ , which describes the motion of thin shell, then its tangent vector  $u^a$  can be written by bulk coordinates

$$u^a = \dot{t}(\partial_t)^a + \dot{r}(\partial_r)^a$$

and its normal vector  $n^a$  has

$$n^a = n^t \left( \frac{\partial}{\partial t} \right)^a + n^r \left( \frac{\partial}{\partial r} \right)^a.$$

Combine  $n^a n_a = 1$  with  $u^a n_a = 0$ , we can obtain

$$n^r = \pm \sqrt{f(r) + \dot{r}^2}, \quad (17)$$

where  $\pm$  determine the direction of  $n^a$ . More specifically, we write  $n^r$  inside and outside the shell as

$$n_o^r = \pm \sqrt{f_+(r) + \dot{r}^2};$$

$$n_i^r = \sqrt{1 + \dot{r}^2}.$$

Notice that the inside spacetime is flat,  $n_i^a$  point to increasing  $r$  in our convention, therefore  $n_i^r$  should be positive.

From (8),(12),(15), one can verify

$$K_i^i = r^{-1} n^r \quad (18)$$

and combine with (11), (12), (13), we conclude the EOM of shell

$$\frac{(D-2)}{8\pi G_D r} \left( (n_i^r - n_o^r) + \frac{2\tilde{\alpha}}{3r^2} (3(1 + \dot{r}^2)(n_i^r - n_o^r) + (n_o^r)^3 - (n_i^r)^3) \right) = S_{\tau\tau} = \sigma. \quad (19)$$

For simplicity, we choose the following units for the rest mass of shell

$$\frac{8\pi G_D}{(D-2)A_{D-2}} = 1,$$

then equation (19) becomes

$$r^{D-3} \left( (n_i^r - n_o^r) + \frac{2\tilde{\alpha}}{3r^2} (3(1 + \dot{r}^2)(n_i^r - n_o^r) + (n_o^r)^3 - (n_i^r)^3) \right) = m, \quad (20)$$

while we have  $(n_i^r)^2 = 1 + \dot{r}^2$  in our case, therefore (20) can be written as

$$r^{D-3} \left( (n_i^r - n_o^r) + \frac{2\tilde{\alpha}}{3r^2} (n_o^r \left( (n_o^r)^2 - 3(n_i^r)^2 \right) + 2(n_i^r)^3) \right) = m. \quad (21)$$

Notice that  $\tilde{\alpha}$  has units  $[L^2]$ . We replace  $r \rightarrow \tilde{\alpha}^{\frac{1}{2}} r$ ,  $m \rightarrow \tilde{\alpha}^{\frac{D-3}{2}} m$ ,  $M \rightarrow \tilde{\alpha}^{\frac{D-3}{2}} M$  and have dimensionless equation

$$r^{D-3} \left( (n_i^r - n_o^r) + \frac{2}{3r^2} (n_o^r \left( (n_o^r)^2 - 3(n_i^r)^2 \right) + 2(n_i^r)^3) \right) = m, \quad (22)$$

while  $f_+(r) = 1 + \frac{r^2}{2} \left( 1 - \sqrt{1 + \frac{16M}{(D-2)r^{D-1}}} \right)$ . In following sections, we always take EOM and  $f_+(r)$  the form which regard  $\{r, m, M\}$  as dimensionless parameters when we refer to EOM and  $f_+(r)$  in specific dimensions.

#### IV. ANALYSIS OF EQUATION OF MOTION FOR THIN SHELL

In this section, we turn to analyze the EOM of spherical shell. The existence of bounce behavior at small radius is firstly given for our spherically symmetric model based on 4D EGB, then we classify the trajectories with bounce behavior into three kinds based on their difference on the Penrose diagram. Finally, we also study the trajectory of thin shell and show the bouncing behavior is absent in higher dimensions. For  $D = 4$ , we make rescaling  $\alpha \rightarrow \frac{1}{D-4}\alpha$ , corresponds to  $\tilde{\alpha} = (D-3)\alpha$ .

##### A. The bouncing process in $D = 4$

Let's show the main results of this paper, namely the bouncing process of dust thin shell. In this subsection,

we restrict to non-extremal cases. Equation (22) can be re-written as

$$\begin{aligned} \dot{r}^6 + \left( \frac{3}{2}r^2 + 3 - \frac{M^2}{m^2} \right) \dot{r}^4 + \left( \frac{3}{4}r^2 + 1 \right)^2 - \frac{9W^2}{64m^2} \\ + \left( \left( \frac{3}{4}r^2 + 2 \right)^2 - 1 - \frac{3MW}{4m^2} \right) \dot{r}^2 = 0, \end{aligned} \quad (23)$$

where

$$\begin{aligned} W = m^2 r + \frac{1}{18} \left( -1 + \sqrt{1 + \frac{8M}{r^3}} \right) r^5 \\ + \frac{4}{9} M \left( 6 + \left( 3 + \sqrt{1 + \frac{8M}{r^3}} \right) r^2 \right). \end{aligned}$$

Eq.(23) is a cubic equation of  $\dot{r}^2$ . According to the discriminant of the cubic algebraic equation, there is a unique real solution for (23) and can simply write it as

$$\dot{r}^2 = V(r, m, M); \quad (24)$$

$$\begin{aligned} V(r, m, M) = \left( -\frac{q}{2} + \sqrt{\left(\frac{q}{2}\right)^2 + \left(\frac{p}{3}\right)^3} \right)^{\frac{1}{3}} \\ + \left( -\frac{q}{2} - \sqrt{\left(\frac{q}{2}\right)^2 + \left(\frac{p}{3}\right)^3} \right)^{\frac{1}{3}} + \frac{M^2}{3m^2} - \frac{1}{2}r^2 - 1, \end{aligned}$$

where

$$\begin{aligned} p = -\frac{M^4}{3m^4} + \frac{(2+r^2)M^2}{m^2} - \frac{3WM}{4m^2} - \frac{3}{16}r^4; \\ q = -\frac{9W^2}{64m^2} + \frac{(-2M^3 + 3m^2M(2+r^2))W}{8m^4} - \frac{2M^6}{27m^6} \\ + \frac{(2+r^2)M^4}{3m^4} - \frac{(16+16r^2+5r^4)M^2}{16m^2} - \frac{r^6}{32} \end{aligned}$$

and  $V(r, m, M) \geq 0$  corresponds to the physical allowable region of the spherical shell trajectory. For illustrating the existence of the bouncing process, without loss of generality, we numerically solve  $V(r) = 0$  for  $M = 5$  with different  $m$  to see the number of turning points in the trajectory of spherical shell, see Figure 1.

To determine the trajectory of bouncing process more specifically, we would follow the analysis method in [36, 37]. The construction of Penrose diagram for 4D EGB black hole (2) is given in Appendix and the meaning of the sign of  $n_o^r$  on the diagram is also illustrated there. Due to  $\sqrt{f_+ + \dot{r}^2} \geq 0$  in equation (22), turning points must locate at the interval which satisfy  $f_+ \geq 0$ , while one can shows  $f_+ < 0$  in  $r_- < r < r_+$ , therefore there is no turning points for thin shell in this interval. Supposing the trajectory of a spherical shell have two turning points which locate at  $0 < r_1 < r_-$  and  $r_2 > r_+$  separately. In this paper, when we refer to an oscillating trajectory, we always mean such a trajectory. We now classify such trajectory into four types on the Penrose diagram. To understand the classification rules, suppose a thin

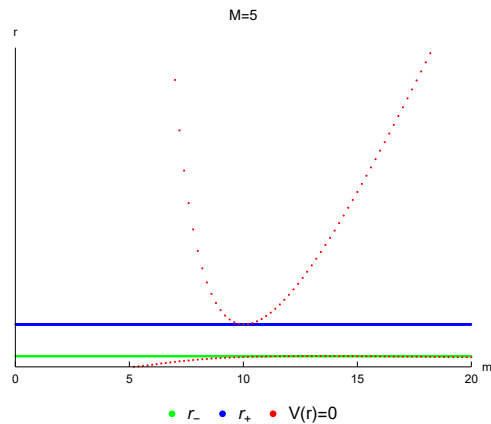


FIG. 1. Equation  $V(r) = 0$  is solved and plotted from  $m = 5$  to  $m = 20$  with step  $\Delta m = 0.2$  for  $M = 5$ . Note that the distance between horizons has been made smaller scale for displaying turning points conveniently.

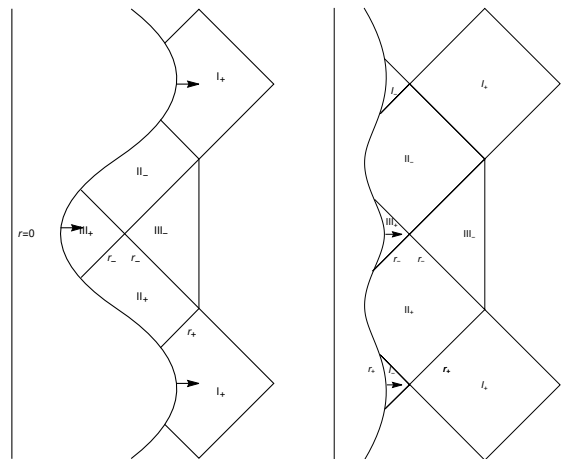


FIG. 2. The left diagram: type *I* oscillating shell. The right diagram: type *IV* oscillating shell.

shell starts in region  $I_+$  in Figure 5, then the worldline of shell will pass region  $II_+$  to reach the minimum  $r_1 < r_-$ . However, there are two possible ways to reach the minimum: entering region  $III_+$  or entering region  $III_-$ . We then give the following two different types of trajectories: type *I* which oscillate between region  $I_+$  and  $III_+$  and type *II* which oscillate between region  $I_+$  and  $III_-$ . Similarly, for the shell which start in region  $I_-$ , its worldline will pass region  $II_+$  and then enter region  $III_+$  or  $III_-$  to reach minimum  $r_1$ , such that we give the other two types of trajectories: type *III* which oscillate between region  $I_-$  and  $III_+$  and type *IV* which oscillate between region  $I_-$  and  $III_-$ . For example, the trajectories of type *I* and type *IV* on the Penrose diagram are shown in Figure 2. We list the four possible oscillation types and the sign of  $n_o^r$  in corresponding region in Table 1.

Now we ask such a question: for an oscillating shell

| Type       | $0 < r \leq r_-$   | $r \geq r_+$     |
|------------|--------------------|------------------|
| <i>I</i>   | $III_+; n_o^r > 0$ | $I_+; n_o^r > 0$ |
| <i>II</i>  | $III_-; n_o^r < 0$ | $I_+; n_o^r > 0$ |
| <i>III</i> | $III_+; n_o^r > 0$ | $I_-; n_o^r < 0$ |
| <i>IV</i>  | $III_-; n_o^r < 0$ | $I_-; n_o^r < 0$ |

TABLE I. The four possible types of oscillation trajectories on the Penrose diagram and the sign of  $n_o^r$  in corresponding region are listed.

with specific mass parameters, which type trajectory it will follow? To answer the question, we first briefly use type *I* trajectory as an example to illustrate our method. Notice that the position of the turning points of the trajectory is decided by (22) with  $\dot{r} = 0$ , specifically, the position of turning points with  $n_o^r > 0$  is given by  $g(r) = 0$ , where

$$g(r) = r \left( 1 - \sqrt{f_+} \right) + \frac{2}{3r} \left( \sqrt{f_+} (-3 + f_+) + 2 \right) - m; \quad (25)$$

Similarly, the position of turning points with  $n_o^r < 0$  is decided by  $h(r) = 0$ , where

$$h(r) = r \left( 1 + \sqrt{f_+} \right) + \frac{2}{3r} \left( -\sqrt{f_+} (-3 + f_+) + 2 \right) - m. \quad (26)$$

Supposing the trajectory of an oscillating shell with mass parameters  $\{m_1, M_1\}$  belongs to type *I* trajectory whose two zero points with  $n_o^r > 0$ . That means  $g(r) = 0$  with  $\{m_1, M_1\}$  must have one zero point at  $0 < r < r_-$  and  $r > r_+$  respectively, then from analyzing the function  $g(r)$ , we will find the existence of such zero points distribution of  $g(r)$  is equivalent to satisfy  $1 < M_1 < m_1 < M_1^-$ , where  $M_1^- = \frac{7}{3}M_1 - \frac{1}{3}\sqrt{M_1^2 - 1}$ . Finally, we conclude the trajectory of the oscillating shell with  $1 < M_1 < m_1 < M_1^-$  is classified in type *I* trajectory. Similar analysis can be done for other type trajectories. In the following, the detailed analysis is given:

The derived function of  $g(r)$  and  $h(r)$  are given by.

$$\begin{aligned} g'(r) &= 1 - \sqrt{f_+} + \frac{1}{r^2} \left( f_+^{-\frac{1}{2}} u \left( f_+ - 1 - \frac{3Mr}{u} \right) \right. \\ &\quad \left. - \frac{2}{3} \left( \sqrt{f_+} (f_+ - 3) + 2 \right) \right); \\ h'(r) &= 1 + \sqrt{f_+} - \frac{1}{r^2} \left( f_+^{-\frac{1}{2}} u \left( f_+ - 1 - \frac{3Mr}{u} \right) \right. \\ &\quad \left. - \frac{2}{3} \left( \sqrt{f_+} (f_+ - 3) - 2 \right) \right), \end{aligned}$$

where  $u = 2(f_+ - 1) - r^2$ . Then the results for the monotonicity of the functions  $g(r)$  and  $h(r)$  in Table 1 are obtained.

In order to analyze the existence of zero points of  $g(r)$  and  $h(r)$ , we list boundary asymptotic behavior of these curves

| Function | $0 < r \leq r_-$ | $r \geq r_+$ | Function | $0 < r \leq r_-$ | $r \geq r_+$ |
|----------|------------------|--------------|----------|------------------|--------------|
| $g'(r)$  | $> 0$            | $< 0$        | $g(r)$   | $\uparrow$       | $\downarrow$ |
| $h'(r)$  | $< 0$            | $> 0$        | $h(r)$   | $\downarrow$     | $\uparrow$   |

TABLE II. The left table: properties of the derivative functions  $g(r)'$  and  $h(r)'$  in  $\{r|r > r_+ \cup r_- > r > 0\}$ . The right table: the monotonicity of the function  $g(r)$  and  $h(r)$ , here  $\uparrow$  means monotonically increasing and  $\downarrow$  means monotonically decreasing.

$$g(r \rightarrow 0) = -(m - M) + \frac{\sqrt{2}M^{\frac{3}{2}}r^{\frac{1}{2}}}{3} + O(r); \quad (27)$$

$$g(r \rightarrow +\infty) = -(m - M) + \frac{M^2}{2r} + O(r^{-2}); \quad (28)$$

$$h(r \rightarrow 0) = \frac{8}{3r} + (-m - M) + O(r^{\frac{1}{2}}); \quad (29)$$

$$h(r \rightarrow +\infty) = 2r + (-m - M) + O(r^{-1}), \quad (30)$$

(a). For  $m > M$ , we can decide the sign of  $g(r)$  and  $h(r)$  at their boundary from their boundary asymptotic behavior. Combined with the monotonicity of the function  $g(r)$  and  $h(r)$  in  $\{r|r > r_+ \cup r_- > r > 0\}$ , the number of zero points for  $g(r)$  and  $h(r)$  in  $\{r|r > r_+ \cup r_- > r > 0\}$  depends on the sign of their value at horizons, then there are four possibilities when there are two turning points for trajectory of thin shell and they show as

$$\{M, m\} = A \cup B \cup C \cup D, \quad (31)$$

where

$$\begin{aligned} A &= \{M, m | m > M \cap g(r_{\pm}) > 0\} \\ &= \{M, m | M \geq 1 \cap M < m < M^-\}; \\ B &= \{M, m | m > M \cap h(r_{\pm}) < 0\} \\ &= \{M, m | M \geq 1 \cap m > M^+\}; \\ C &= \{M, m | m > M \cap h(r_-) < 0 \cap g(r_+) > 0\} = \phi; \\ D &= \{M, m | m > M \cap h(r_+) < 0 \cap g(r_-) > 0\} \\ &= \{M, m | M > 1 \cap M^- < m < M^+\}, \end{aligned}$$

where  $M^+ = \frac{7M}{3} + \frac{1}{3}\sqrt{M^2 - 1}$ . Now we conclude the trajectory of oscillating shell with mass parameters A/B/D is type I/IV/III trajectory, while type II trajectory is absent. Intuitively, we use the left diagram of Figure 3 to show the classification in mass parameters' space. Specially, at the mass parameter  $\{M = 1, m = \frac{7}{3}\}$ , we also find the EOM can describe a static configuration of the spherical shell, which forms an extremal black hole for an outside observer, and the shell locates exactly at the radial position of the horizon, as the right diagram of Figure 3 shows.

Until now, we have classified the oscillating thin shell on Penrose diagram into three cases, which means we can infer the interval of the shell's mass parameter by understanding the trajectory of oscillating shell on the

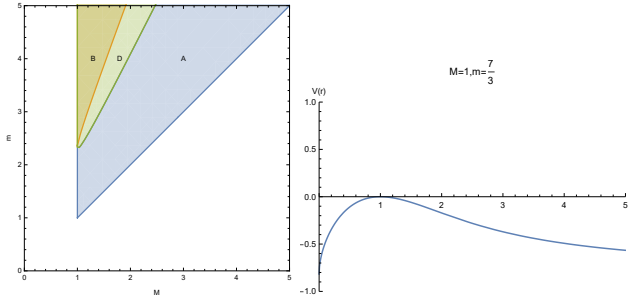


FIG. 3. The left diagram: the classifications of bouncing processes by different mass parameters' regions. The right diagram: the  $V(r)$  profile of  $\{M = 1, m = \frac{7}{3}\}$ , which corresponds to the intersection of region  $A, B, D$  of left diagram. It shows that the spherical shell locate at  $r = 1$  where the position of horizon of extremal black hole is.

Penrose diagram. Physically, we are actually interested is the type I trajectory, whose mass parameters correspond to the region  $A$  in Figure 3, because it's observable for the asymptotic observer of region  $I_+$  on the Penrose diagram, which is not the case for type  $III, IV$  trajectory, see Figure 2.

(b). For  $m \leq M$ , we have  $g(r \rightarrow 0) > 0$  and  $g(r \rightarrow +\infty) > 0$ . According to the monotonic property and asymptotic behavior of  $g(r)$  in  $\{r | r > r_+ \cup r_- > r > 0\}$ , one can conclude  $g(r)$  has no zero point, which means the trajectory of spherical shell doesn't has turning point with  $n_o^r > 0$ . It also can be proved that there is no turning point with  $n_o^r < 0$  at the trajectory of the spherical shell in this mass interval. Supposing we have such turning point, it's equivalent to the mass parameters should have either  $\{M, m | h(r_+) < 0\} = \{M, m | M \geq 1 \cap m > \frac{7M}{3} - \frac{1}{3}\sqrt{M^2 - 1}\}$  or  $\{M, m | h(r_-) < 0\} = \{M, m | M \geq 1 \cap m > \frac{7M}{3} + \frac{1}{3}\sqrt{M^2 - 1}\}$ , which intersect with  $m \leq M$  is the empty set, therefore we infer that the turning point of trajectory of shell with  $n_o^r < 0$  is absent. Now we have proved that trajectory of shell with  $m \leq M$  doesn't has turning point, ie. the ultimate fate of collapsing spherical shell with  $m \leq M$  would collapse into a singularity.

## B. Higher dimensions

Now we study the trajectory of thin shell in higher dimensions. In this case, there is generally always one and only one horizon  $r_H$  and the position of horizon  $f_+ = 0$  gives  $r^{D-5}(1+r^2) = \frac{4M}{D-2}$ . For  $D > 5$ , the left-hand side is monotonically increasing from zero to infinity, therefore there exist only one solution. For  $D = 5$ , the existence of horizon depends on the sign of  $\frac{4}{3}M - 1$  and there exist one horizon when  $M > \frac{3}{4}$ , which we consider here.

Physically, we believe that the existence of bouncing behavior in four dimensions is due to its special causal

structure compared with higher dimensions' case. In fact, since the Gauss-Bonnet term modify the small scale behavior of the Einstein gravity, while the turning point of spherical shell in higher dimensions locate outside the horizon of outer spacetime, it's reasonable to speculate the number of turning points for shell's trajectory in high dimensions should be the same. For this reason, without loss of generality, we gives the analysis for EGB case in five dimensions.

In this subsection, we are interested in the trajectory of shell with  $n_o^r > 0$  in  $r > r_H$ . To decide the location of turning point of shell's trajectory, which is given by

$$r^2 \left( (1 - \sqrt{f_+}) + \frac{2}{3r^2} (\sqrt{f_+}(-3 + f_+) + 2) \right) = m,$$

is equivalent to find zero points of

$$G(r) = r^2 (1 - \sqrt{f_+}) + \frac{2}{3} (\sqrt{f_+}(-3 + f_+) + 2) - m,$$

whose derived function is given by

$$G'(r) = 2r (1 - \sqrt{f_+}) + \frac{1}{\sqrt{f_+}r} \left( (f_+ - 1)(2(f_+ - 1) - r^2) - \frac{8}{3}M \right),$$

and asymptotic behavior at infinity is

$$G(r \rightarrow +\infty) = \left( -m + \frac{2}{3}M \right) + \frac{2}{9}M^2r^{-2} + O(r^{-3}).$$

Through the analysis of the derivative function, we can see  $G(r)$  is monotonically decreasing in  $r > r_H$ , which means there exist zero point for  $G(r)$  in this interval only and only if the mass parameters satisfy

$$\begin{aligned} \{m, M\} &= \{G(r_H) > 0 \cap G(+\infty) < 0\} \\ &= \left\{ \frac{2}{3}M < m \leq \frac{1}{3}(1 + 4M) \right\}. \end{aligned} \quad (32)$$

However, we cannot generally deduce which type of turning point is in this case, is it expanding shell with mass parameters (32) cannot escape from its own gravitational pull or collapsing shell bounce back to infinity? Nevertheless we still can numerically decide which type of the turning point for some specific mass parameters. Transforming (22) in five dimensions and obtain

$$\begin{aligned} r^6 + \left( \frac{3}{2}r^2 + 3 - \frac{4M^2}{9m^2} \right) r^4 + \left( \frac{3}{4}r^2 + 1 \right)^2 - \frac{9Q^2}{64m^2} \\ + \left( \left( \frac{3}{4}r^2 + 2 \right)^2 - 1 - \frac{MQ}{2m^2} \right) r^2 = 0, \end{aligned} \quad (33)$$

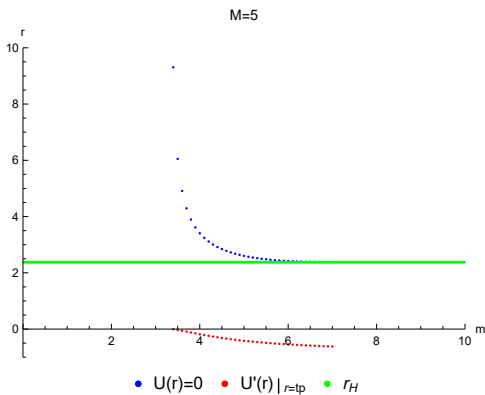


FIG. 4. The location of turning points for  $M = 5$  with  $m$  from 3.4 to 7 with  $\Delta m = 0.1$  is plotted. Note that  $U'(r)|_{r=tp}$  has only numerical meaning in the vertical direction.

where

$$Q = m^2 + \frac{1}{18} \left( -1 + \sqrt{1 + \frac{16M}{3r^4}} \right) r^6 + \frac{8}{27} M \left( 6 + \left( 3 + \sqrt{1 + \frac{16M}{3r^4}} \right) r^2 \right).$$

Like the case of four dimensions, one can find there is a unique real solution for (33), which denotes  $\dot{r}^2 = U(r, m, M) = V(r, \frac{m}{r}, \frac{2M}{3r})$ , where  $U(r, m, M) \geq 0$  corresponds to the physical allowable region of the spherical shell trajectory. Without loss of universality, we take  $M = 5$  with different  $m$  which satisfy (32) to solve  $U(r) = 0$  to see the location of turning point of trajectory of spherical shell, which we denote  $r_{tp}$ , and study the sign of  $U'(r_{tp})$  to see the force at this position, see Figure 4. It can be seen from Figure 4 that the direction of force of spherical shell at these turning points is pointing to decreasing  $r$ , which means the spherical shell with these mass parameters cannot escape from its own gravitational pull.

In summary, we conclude that collapsing thin shell has novel bouncing process in four dimensions, while higher dimensions' case seems absent, as confirmed by the detailed analysis in five dimensions. The bouncing behavior is indeed caused by the  $\alpha$  term in four dimensions, whose effect is similar to electrical charge somehow, regardless it contribute to the Einstein theory as pure gravitational correction.

## V. WEAK COSMIC CENSORSHIP FOR THIN SHELL

The cosmic censorship has been tested by thin shell for many years. In Schwarzschild spacetime, we know that there always exist horizon for  $M > 0$ . For 4D EGB gravity, from equation (2), we can infer that only  $M \geq \alpha$  makes the appearance of horizon and  $M < \alpha$  which

we refer to underweighted spacetime later describes spacetime with naked singularity such that it's natural to ask, can a shell with underweighted exterior ( $M < \alpha$ ) implode past the horizons of an existing non-extremal black hole ( $M > \alpha$ )? If it does, then a singularity forms and the violation of weak cosmic censorship happens. Next we turn to construct this scenario to test the cosmic censorship conjecture.

In this section, we are concentrated on the the asymptotically flat region, where  $n^r > 0$  is always true. For our purpose, we consider such a process of gravitational collapse for spherical shell, whose both interior and exterior geometry are given by the spherical symmetric solution (1). Let  $M_i$  and  $M_o$  denotes the interior and exterior mass parameter and we have

$$F_i(r) = 1 + \frac{r^2}{2\alpha} \left( 1 - \sqrt{1 + \frac{8\alpha M_i}{r^3}} \right);$$

$$F_o(r) = 1 + \frac{r^2}{2\alpha} \left( 1 - \sqrt{1 + \frac{8\alpha M_o}{r^3}} \right),$$

while we set  $M_i > \alpha$  and  $M_o < \alpha$ . The motion of spherical shell obeys (20) which we have obtained before, we transform (20) in four dimensions and obtain

$$r(n_i^r - n_o^r) \left( 1 + \frac{2\alpha}{3r^2} (3(1 + \dot{r}^2) - ((n_o^r)^2 + n_o^r n_i^r + (n_i^r)^2)) \right) = m, \quad (34)$$

where

$$n_i^r = \sqrt{F_i(r) + \dot{r}^2}; \quad n_o^r = \sqrt{F_o(r) + \dot{r}^2}.$$

Since  $F(r)$  ranges monotonically decreasing from  $M = 0$  to  $M = +\infty$ , therefore we have  $F_o(r) > F_i(r)$  and  $n_o^r > n_i^r$  further. Combined with  $0 < n_i^r < n_o^r < \sqrt{1 + \dot{r}^2}$ , the left-hand side of (34) has

$$r(n_i^r - n_o^r) \left( 1 + \frac{2\alpha}{3r^2} (3(1 + \dot{r}^2) - ((n_o^r)^2 + n_o^r n_i^r + (n_i^r)^2)) \right) < r(n_i^r - n_o^r) < 0, \quad (35)$$

which means  $m$  in (34) should be negative. However, the weak energy condition of (13) tell us  $\sigma(\tau) > 0$ , which is identified with  $m > 0$ , such that (34) with these parameters is unphysical. In other words, it can't violate the cosmic censorship through dynamics of thin shell in 4D EGB gravity and the cosmic censorship conjecture holds. Moreover, the above analysis also applies to test the third law of black hole dynamics, namely the extremal black hole never forms. The only change for above discussion that needs to be done is replace the outer spacetime with extremal black hole which has  $M = \alpha$ , then one will find the law also still hold in this scenario.

## VI. CONCLUDING REMARKS

In this paper, we have considered gravitational collapse of dust thin shell in EGB gravity. We have derived the



equations of motion for a massive spherical thin shell in  $D$  dimensions. Based on the newly proposed 4D EGB gravity, we are motivated by the trajectory of collapsing dust star and find there exists novel bouncing behavior for the thin shell in small scale on the Penrose diagram. It is worth to note that the bouncing process is consistent with the fact that the higher curvature corrections to GR modifies the small scale behavior of Einstein's gravity. We analyze the EOM in four dimensions and classify the oscillating shell on the Penrose diagram. The analysis of EOM for higher dimensions is also given, where it turns out that the collapsing thin shell will not be bounced back at a small radius (i.e. the singularity always forms). Finally, we test the weak cosmic censorship conjecture and find that it still holds in our model. However, there are still some questions to be answered. Is the oscillation behavior still true for more realistic cases, such as thick shells, shells with more realistic equations of state and general (non-)spherical stars? Can dissipation during the collapse be taken into account? What will happen then? These questions will be left for future works.

### ACKNOWLEDGMENTS

We are grateful to Hongbao Zhang for his helpful discussions. This work is partially supported by NSFC with Grant No.11975235, 12035016, 11731001 and 11575286.

## VII. APPENDIX

### A. The Penrose diagram of 4D EGB black hole

The Penrose diagram is a crucial tool for analyzing spacetime in GR. We now construct the Penrose diagram of the spherically symmetric vacuum solution for 4D EGB gravity (2).

In this section, we are interested in the non-extremal case. The metric (2) is singular when  $r = 0, r_{\pm}$ . Cutting the spacetime manifold into three disconnected regions in the coordinates  $\{t, r, \theta, \phi\}$  and they are  $0 < r < r_-$ ,  $r_- < r < r_+$  and  $r_+ < r < +\infty$  separately. Since we consider the connected spacetime manifold, we choose the region  $r_+ < r < +\infty$  initially, which is named region  $I_+$  later and represent the external field. It can be showed the region is extensible.

Let's introduce null coordinates  $U, V$  in region  $I_+$ , which denotes

$$V = \exp(t + r_*); \quad U = -\exp(r_* - t),$$

where the tortoise coordinate  $r_*$  is defined by  $r_* = \int dr F(r)^{-1}$ . Note that we have

$$\begin{aligned} \lim_{r \rightarrow +\infty} r_* &= +\infty; & \lim_{r \rightarrow r_+} r_* &= -\infty; \\ \lim_{r \rightarrow r_-} r_* &= +\infty; & \lim_{r \rightarrow 0} r_* &= c, \end{aligned}$$

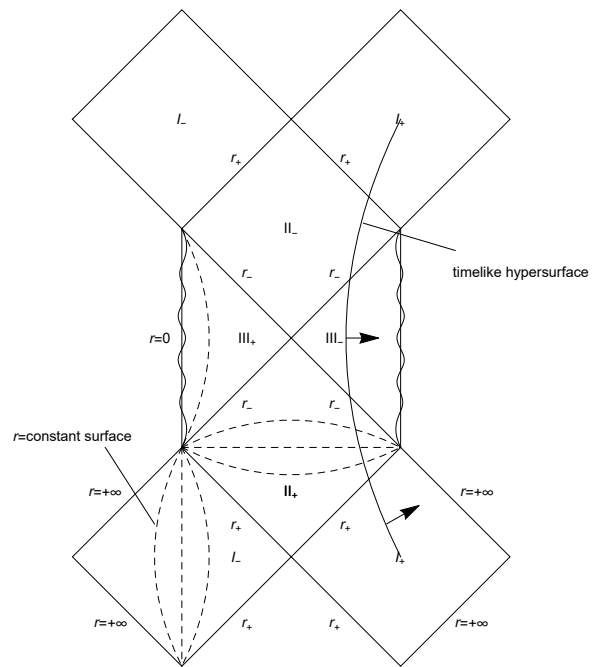


FIG. 5. The Penrose diagram of 4D EGB vacuum solution with  $M > \alpha$ .

where  $c$  is a constant.

Using the coordinates  $\{U, V, \theta, \phi\}$ , the metric (2) takes the form

$$ds^2 = F(r) \exp(-2r_*) dU dV + r^2 (d\theta^2 + \sin^2 \theta d\phi^2). \quad (36)$$

One can prove (36) is no longer singular at  $r = r_+$ . This suggests actually the singularity  $r = r_+$  is a result of bad choice of coordinates, it's not real singularity.

Next we use the arctangent to bring  $U, V$  into a finite coordinate value and define

$$V' = \arctan V; \quad U' = \arctan U. \quad (37)$$

For region  $I_+$ , its corresponding ranges given by

$$0 < V' < \frac{\pi}{2}; \quad -\frac{\pi}{2} < U' < 0,$$

and because  $r = r_+$  is non-singular, it's naturally extend the region  $I_+$  across  $r = r_+$  to a new region which is isometric to the region  $r_- < r < r_+$  of the 4D EGB solution (2), either along the direction of  $\partial_{U'}$  or  $\partial_{V'}$ . For the direction of  $\partial_{U'}$ , the new region called region  $II_+$  is parameterized by

$$0 < V' < \frac{\pi}{2}; \quad 0 < U' < \frac{\pi}{2}.$$

Together with  $r = r_+$ , region  $I_+$  and  $II_+$ , we obtain Penrose diagram of the region  $r_- < r < +\infty$  for (2).

Similarly, one can find  $r_-$  is also not a real singularity so that one can extend region  $r_- < r < r_+$  to region  $0 < r < r_-$ , which we called region  $III_+$ . Extend the

diagram along direction  $\partial_U$  or  $\partial_V$  continually like RN case, the extended Penrose diagram of 4D EGB solution is obtained, see Figure 5.

Now we introduce a timelike hypersurface to illustrate the meaning of the sign of  $n_o^r$  on the Penrose diagram. In our convention, its normal vector  $n_o^a$  is pointing from inside to outside, as the arrow in Figure 5 shows. The

sign of  $n_o^r$  depends on the direction of  $n_o^a$  pointing. If  $n_o^a$  points to larger  $r$ , then we have  $n_o^r > 0$ , while  $n_o^a$  points to smaller  $r$  means  $n_o^r < 0$ . Notice that the sign of  $n_o^r$  vary from region to region. For instance, in region  $I_+$ ,  $n_o^a$  always points to larger  $r$  so that  $n_o^r > 0$ , while  $n_o^a$  always points to smaller  $r$  in region  $III_-$ , therefore  $n_o^r < 0$ .

- 
- [1] Dražen Glavan and Chunshan Lin. Einstein-Gauss-Bonnet Gravity in Four-Dimensional Spacetime. *Phys. Rev. Lett.*, 124(8):081301, 2020.
- [2] Rong-Gen Cai, Li-Ming Cao, and Nobuyoshi Ohta. Black Holes in Gravity with Conformal Anomaly and Logarithmic Term in Black Hole Entropy. *JHEP*, 04:082, 2010.
- [3] Daniele Malafarina, Bobir Toshmatov, and Naresh Dadhich. Dust collapse in 4D Einstein-Gauss-Bonnet gravity. *Phys. Dark Univ.*, 30:100598, 2020.
- [4] Pedro G. S. Fernandes. Charged Black Holes in AdS Spaces in 4D Einstein Gauss-Bonnet Gravity. *Phys. Lett. B*, 805:135468, 2020.
- [5] Shao-Wen Wei and Yu-Xiao Liu. Testing the nature of Gauss-Bonnet gravity by four-dimensional rotating black hole shadow. 3 2020.
- [6] Rahul Kumar and Sushant G. Ghosh. Rotating black holes in 4D Einstein-Gauss-Bonnet gravity and its shadow. *JCAP*, 07(07):053, 2020.
- [7] Sushant G. Ghosh and Sunil D. Maharaj. Radiating black holes in the novel 4D Einstein-Gauss-Bonnet gravity. *Phys. Dark Univ.*, 30:100687, 2020.
- [8] R. A. Konoplya and A. Zhidenko. Black holes in the four-dimensional Einstein-Lovelock gravity. *Phys. Rev. D*, 101(8):084038, 2020.
- [9] Kartheek Hegde, A. Naveena Kumara, C. L. Ahmed Rizwan, Ajith K. M., and Md Sabir Ali. Thermodynamics, Phase Transition and Joule Thomson Expansion of novel 4-D Gauss Bonnet AdS Black Hole. 3 2020.
- [10] Shao-Wen Wei and Yu-Xiao Liu. Extended thermodynamics and microstructures of four-dimensional charged Gauss-Bonnet black hole in AdS space. *Phys. Rev. D*, 101(10):104018, 2020.
- [11] Minyong Guo and Peng-Cheng Li. Innermost stable circular orbit and shadow of the 4D Einstein-Gauss-Bonnet black hole. *Eur. Phys. J. C*, 80(6):588, 2020.
- [12] Rahul Kumar, Shafqat Ul Islam, and Sushant G. Ghosh. Gravitational lensing by charged black hole in regularized 4D Einstein-Gauss-Bonnet gravity. *Eur. Phys. J. C*, 80(12):1128, 2020.
- [13] Akash K. Mishra. Quasinormal modes and strong cosmic censorship in the regularised 4D Einstein-Gauss-Bonnet gravity. *Gen. Rel. Grav.*, 52(11):106, 2020.
- [14] R. A. Konoplya and A. F. Zinhailo. Quasinormal modes, stability and shadows of a black hole in the 4D Einstein-Gauss-Bonnet gravity. *Eur. Phys. J. C*, 80(11):1049, 2020.
- [15] Cheng-Yong Zhang, Shao-Jun Zhang, Peng-Cheng Li, and Minyong Guo. Superradiance and stability of the regularized 4D charged Einstein-Gauss-Bonnet black hole. *JHEP*, 08:105, 2020.
- [16] Cheng Liu, Tao Zhu, and Qiang Wu. Thin Accretion Disk around a four-dimensional Einstein-Gauss-Bonnet Black Hole. *Chin. Phys. C*, 45(1):015105, 2021.
- [17] C. Y. Zhang, P. C. Li and M. Guo, *Eur. Phys. J. C* **80** (2020) no.9, 874 doi:10.1140/epjc/s10052-020-08448-z [arXiv:2003.13068 [hep-th]].
- [18] R. A. Hennigar, D. Kubizňák, R. B. Mann and C. Pollack, *JHEP* **07** (2020), 027 doi:10.1007/JHEP07(2020)027 [arXiv:2004.09472 [gr-qc]].
- [19] Wen-Yuan Ai. A note on the novel 4d einstein-gauss-bonnet gravity. *Communications in Theoretical Physics*, 72(9):095402, aug 2020.
- [20] Naresh Dadhich. On causal structure of 4D-Einstein-Gauss-Bonnet black hole. *Eur. Phys. J. C*, 80(9):832, 2020.
- [21] J. Arrechea, A. Delhom and A. Jiménez-Cano, *Phys. Rev. Lett.* **125** (2020) no.14, 149002 doi:10.1103/PhysRevLett.125.149002 [arXiv:2009.10715 [gr-qc]].
- [22] Metin Gurses, Tahsin Cagri Sisman, and Bayram Tekin. Comment on "Einstein-Gauss-Bonnet Gravity in 4-Dimensional Space-Time". *Phys. Rev. Lett.*, 125(14):149001, 2020.
- [23] Metin Gurses, Tahsin Cagri Sisman, and Bayram Tekin, *Eur. Phys. J. C* **80**, no.7, 647 (2020) doi:10.1140/epjc/s10052-020-8200-7 [arXiv:2004.03390 [gr-qc]].
- [24] D. Christodoulou, *Commun. Math. Phys.* **93** (1984), 171-195 doi:10.1007/BF01223743
- [25] R. P. A. C. Newman, *Class. Quant. Grav.* **3** (1986), 527-539 doi:10.1088/0264-9381/3/4/007
- [26] A. Banerjee, U. Debnath and S. Chakraborty, *Int. J. Mod. Phys. D* **12** (2003), 1255-1264 doi:10.1142/S021827180300375X [arXiv:gr-qc/0211099 [gr-qc]].
- [27] R. Goswami and P. S. Joshi, *Phys. Rev. D* **69** (2004), 044002 doi:10.1103/PhysRevD.69.044002 [arXiv:gr-qc/0212097 [gr-qc]].
- [28] H. Maeda, *Phys. Rev. D* **73** (2006), 104004 doi:10.1103/PhysRevD.73.104004 [arXiv:gr-qc/0602109 [gr-qc]].
- [29] S. Jhingan and S. G. Ghosh, *Phys. Rev. D* **81** (2010), 024010 doi:10.1103/PhysRevD.81.024010 [arXiv:1002.3245 [gr-qc]].
- [30] S. G. Ghosh and S. Jhingan, *Phys. Rev. D* **82** (2010), 024017 doi:10.1103/PhysRevD.82.024017 [arXiv:1004.0071 [gr-qc]].
- [31] K. Zhou, Z. Y. Yang, D. C. Zou and R. H. Yue, *Mod. Phys. Lett. A* **26** (2011), 2135-2147 doi:10.1142/S0217732311036449 [arXiv:1107.2728]

- [gr-qc]].
- [32] Farrugia, C. J., Hajicek, P. 1979. The third law of black hole mechanics: A counterexample. *Communications in Mathematical Physics* 68, 291-299. doi:10.1007/BF01221129.
- [33] W. Israel, *Phys. Rev. Lett.* **57** (1986) no.4, 397 doi:10.1103/PhysRevLett.57.397.
- [34] R. M. Wald, doi:10.1007/978-94-017-0934-7\_5 [arXiv:gr-qc/9710068 [gr-qc]].
- [35] V. E. Hubeny, *Phys. Rev. D* **59** (1999), 064013 doi:10.1103/PhysRevD.59.064013 [arXiv:gr-qc/9808043 [gr-qc]].
- [36] David G. Boulware. Naked Singularities, Thin Shells, and the Reissner-Nordström Metric. *Phys. Rev. D*, 8(8):2363, 1973.
- [37] Sijie Gao and Jose P. S. Lemos. Collapsing and static thin massive charged dust shells in a Reissner-Nordstrom black hole background in higher dimensions. *Int. J. Mod. Phys. A*, 23:2943–2960, 2008.
- [38] D. G. Boulware and S. Deser, *Phys. Rev. Lett.* **55** (1985), 2656 doi:10.1103/PhysRevLett.55.2656.
- [39] S. C. Davis, *Phys. Rev. D* **67** (2003), 024030 doi:10.1103/PhysRevD.67.024030 [arXiv:hep-th/0208205 [hep-th]].
- [40] C. S. Chu and H. S. Tan, [arXiv:2103.06314 [hep-th]].